Acta Crystallographica Section D
**Biological Crystallography**
ISSN 0907-4449

# Structure of a superoxide dismutase and implications for copper-ion chelation

**Manickam Yogavel,[a] Prakash Chandra Mishra,[a] Jasmita Gill,[a] Pardeep Kumar Bhardwaj,[b] Som Dutt,[b] Sanjay Kumar,[b] Paramvir Singh Ahuja[b] and Amit Sharma[a]***

[a]Structural and Computational Biology Group, International Centre for Genetic Engineering and Biotechnology, Aruna Asaf Ali Road, New Delhi 110 067, India, and [b]Division of Biotechnology, Institute of Himalayan Bioresource Technology, Palampur (HP), India

Correspondence e-mail: asharma@icgeb.res.in

Received 29 April 2008
Accepted 24 June 2008

**PDB Reference:** superoxide dismutase, 2q2l, r2q2lsf.

Superoxide dismutase (SOD) plays a central role in cellular defence against oxidative stress and is of pharmaceutical importance. The SOD from *Potentilla atrosanguinea* (Pa-SOD) is a unique enzyme as it possesses free-radical scavenging capability at temperatures ranging between 263 and 353 K. The crystal structure of recombinant Pa-SOD has been determined to 2.3 Å resolution. The active-site residues are well ordered and additional water molecules are present in place of a bound copper ion. There is a significant difference in the relative orientation of the two subunits of Pa-SOD and asymmetry is also present in numerous hydrogen-bonding interactions. Structures of SODs, both bound with copper and unbound, have been compared with respect to the orientation of the electrostatic and Greek-key loops. This analysis provides new insights into the copper-chelation process in SODs. Several new structural features in Pa-SOD which may be responsible for its unique properties of thermostability and expanded range of antioxidant activity are also highlighted.

## 1. Introduction

Copper/zinc superoxide dismutase (CuZnSOD) removes oxygen radicals in cells by catalyzing their breakdown into hydrogen peroxide and water (Bannister *et al.*, 1987). CuZnSOD has to undergo several post-translational modifications before becoming active: the protein requires the addition of Zn and Cu ions, followed by the formation of a conserved disulfide. Analysis of the crystal structures of CuZnSODs from eukaryotic species [*Bos taurus* (Bt-SOD), *Spinacia oleracea* (So-SOD), *Saccharomyces cervisiae* (Sc-SOD), *Homo sapiens* (Hs-SOD), *Xenopus laevis* (Xl-SOD) and *Schistosoma mansoni* (Sm-SOD); Tainer *et al.*, 1982; Kitagawa *et al.*, 1991; Djinović *et al.*, 1992; Parge *et al.*, 1992; Carugo *et al.*, 1996; Cardoso *et al.*, 2004] and several prokaryotic species (*Photobacterium leiognathi*, *Escherichia coli*, *Actinobacillus pleuropneumoniae*, *Salmonella typhimurium* and *Mycobacterium tuberculosis*; Pesce *et al.*, 1997, 2000; Forest *et al.*, 2000; Spagnolo *et al.*, 2004) has shown that all these CuZnSODs display a conserved three-dimensional fold built on a flattened Greek-key motif (eight-stranded $\beta$-barrel; Bordo *et al.*, 2001). The eukaryotic and prokaryotic CuZnSODs have similar dimensions ($\sim$60 $\times$ 30 $\times$ 30 and $\sim$70 $\times$ 30 $\times$ 30 Å, respectively) and are homodimeric, with a twofold-symmetry axis along the $\beta$-barrel axis. This dimeric SOD structure maintains the orientation of the two active sites within each dimer. However, the prokaryotic CuZnSODs are characterized by a quaternary structure that is distinct from that of the eukaryotic enzymes (Pesce *et al.*, 1997) in terms of interface residues. The binuclear (Zn and Cu) active-site metal

**Table 1**
Diffraction data and structure-refinement statistics.

| | |
|---|---|
| PDB code | 2q2l |
| Data collection | |
| Space group | *C*2 |
| Unit-cell parameters (Å, °) | $a$ = 89.14, $b$ = 64.12, $c$ = 63.62, $\beta$ = 124.33 |
| Resolution range (Å) | 50.0–2.36 (2.44–2.36) |
| Unique reflections | 10953 (526) |
| Completeness (%) | 94.4 (63.6) |
| $I/\sigma(I)$ | 32.7 (6.0) |
| $R_{\rm merge}$ | 0.054 (0.149) |
| Multiplicity | 6.3 (3.3) |
| Refinement | |
| Reflections in working set | 10953 |
| Reflections in test set (4.7%) | 546 |
| $R$ factor/$R_{\rm free}$ (%) | 16.9/23.7 |
| Model compositions | |
| Amino acids (*A* and *B* chains) | 304 |
| No. of protein atoms (No. with partial occupancy) | 2230 (196) |
| Zn ions | 2 |
| Iodides | 10 |
| Water molecules | 203 |
| Stereochemistry | |
| Bond lengths (Å) | 0.01 |
| Bond angles (°) | 1.5 |
| Ramachandran plot | |
| Residues in most favoured regions (%) | 87.3 |
| Residues in additional allowed regions (%) | 12.7 |
| Mean $B$ factors (Å$^2$) | |
| Main-chain atoms | 23.6 |
| Side-chain atoms | 23.5 |
| Zn ions | 21.9 |
| Iodides | 30.4 |
| Water molecules | 27.5 |

centres sit on the $\beta$-barrel surrounded by surface protein loops. Active SOD contains one zinc ion and one copper ion per subunit. Little is known on how SOD acquires the zinc ion; however, copper insertion is likely to be assisted by a copper metallochaperone called copper chaperone for superoxide dismutase (CCS; Culotta *et al.*, 1997; Portnoy *et al.*, 2001; Lamb *et al.*, 2001; Banci, Bertini, Cantini *et al.*, 2002; Banci, Bertini, Cramaro *et al.*, 2002; Furukawa *et al.*, 2004; Banci *et al.*, 2006).

*Potentilla atrosanguinea* grows abundantly at Kunzum Pass (altitude 4517 m), Himachal Pradesh in the Western Himalayas, India. The light intensity in this area is 2500 µeinstein m$^{-2}$ s$^{-1}$ and the daytime air temperature is 276–283 K. Interestingly, no other plant grows as luxuriantly at Kunzum Pass. Such an environment of low temperature coupled with high light intensity would lead to the generation of superoxide anions ($O_2^-$) within the plant cells at a very high rate (Allen, 1995). The plant therefore requires the capability to dismutate $O_2^-$ in order to survive and complete its life cycle. In line with this, the SOD from *P. atrosanguinea* (Pa-SOD) has free-radical scavenging activity between 263 and 353 K and is also autoclavable at 394 K (Kumar *et al.*, 2002). Owing to the properties mentioned above, Pa-SOD has utility in the medical, cosmetic and food industries. It may also be valuable for producing transgenic plants which need additional resistance/tolerance to biotic and abiotic stresses.

Most hyperthermophiles studied to date belong to the kingdom of archaea and only two families, *Thermotoga* and *Aquifex*, are bacterial (Nesbo *et al.*, 2001). Considerable data exist on the structural features that may assist in the thermal stability of proteins from hyperthermophiles. The maximum thermostability of SOD reported to date is at 353 K and the minimum temperature reported for the catalysis of dismutation is 278 K (Hakam & Simon, 1996). However, increased thermostability and a lowered temperature for the catalysis of dismutation of $O_2^-$ have only been reported in the same enzyme for Pa-SOD (Kumar *et al.*, 2002). Pa-SOD is the only case study to date in which the enzyme can catalyze the dismutation of $O_2^-$ at temperatures below 273 K and can also be autoclaved.

This study reports the crystal structure analysis of Pa-SOD at 2.3 Å resolution. The structure was solved using the iodide-SAD method described previously (Yogavel *et al.*, 2007). A comparative structural analysis of seven eukaryotic CuZn-SODs revealed four distinct stages of copper chelation. Based on our and earlier SOD structures, protein conformations have been studied in the copper-unbound state, in the early copper-harbouring stage, in the intermediate stage and finally in the fully bound form. An in-depth analysis of copper loading onto SODs provided insights into the copper-binding process. Using the copper-unbound structure (Pa-SOD), the early copper-harbouring stage (So-SOD), the intermediate copper-harbouring stage (Sm-SOD, Sc-SOD and Xl-SOD) and the fully loaded stage (Hs-SOD and Bt-SOD), we are able propose a copper-binding mechanism for this family of enzymes. We also highlight several unique properties of Pa-SOD that may contribute to its thermostability.

## 2. Materials and methods

### 2.1. Purification of Pa-SOD

Bacterial strain M15 cells transformed with PA-SOD-pQE30 plasmid were grown in LB containing 30 µg ml$^{-1}$ kanamycin and 100 µg ml$^{-1}$ ampicillin. The bacterial culture was induced using 1 m*M* IPTG (at an OD of 0.6) and grown for a further 4 h post-induction. The cell pellet obtained after centrifugation was lysed using a sonicator (buffer: 50 m*M* Tris pH 8.00, 300 m*M* NaCl, 1 m*M* DTT, 0.1 mg ml$^{-1}$ lysozyme, 1 m*M* PMSF, 10 m*M* imidazole supplemented with EDTA-free protease-inhibitor cocktail). The supernatant obtained by centrifugation at 23 400*g* for 45 min was passed through Ni–NTA beads. The beads were washed with buffer (50 m*M* Tris pH 8.00, 300 m*M* NaCl, 1 m*M* DTT, 1 m*M* PMSF, 20 m*M* imidazole) and the protein was eluted using imidazole. The protein was further purified using ion-exchange and gel-filtration chromatography. The purified protein was buffer-exchanged into 25 m*M* Tris pH 7.5, 25 m*M* NaCl, 1 m*M* DTT and 0.02% sodium azide and concentrated to 10 mg ml$^{-1}$. No external copper or zinc were added to the Pa-SOD during the purification procedure.

### 2.2. Crystallization and data collection

Crystals of Pa-SOD were obtained at 293 K by the hanging-drop vapour-diffusion method using 0.2 *M* ammonium iodide and 20% PEG 3350 as precipitant. A needle-shaped crystal

was soaked for a short period (~30 s) in a cryoprotectant solution which consisted of the mother liquor supplemented with 20% ethylene glycol. Data were collected at 100 K using Cu $K\alpha$ radiation ($\lambda$ = 1.54 Å) generated by a Micro-Max 007 rotating-anode X-ray generator (Rigaku/MSC) operated at 40 kV and 20 mA with Osmic mirrors (Vari Max HR). Diffraction images were recorded using a MAR345dtb (MAR Research Inc.) image-plate detector. Data integration and scaling were carried out using the *HKL*-2000 suite (Otwinowski & Minor, 1997). Data statistics are reported in Table 1.

### 2.3. Structure solution and refinement

Details of structure solution followed by partial refinement have been published previously (Yogavel *et al.*, 2007). In brief, the structure was solved by single-wavelength anomalous diffraction by exploiting the anomalous signal of iodide ions, which have $f'' = 6.8$ electrons at the home-source Cu $K\alpha$ wavelength (1.54 Å). The mean anomalous signal-to-noise ratio [$|\Delta F|/\sigma(\Delta F)$] in the SAD data we collected was 2.13 and was significant to ~3.0 Å resolution. The anomalous scatterers were located with *AutoSol* (Adams *et al.*, 2002) using a 3.0 Å resolution cutoff. Ten iodide ions were obtained with a figure of merit (FOM) of 0.33 and a preliminary model was built automatically. The partial model obtained from *AutoSol* in *PHENIX* was fed into *AutoBuild* for iterative model building and refinement, resulting in a model containing 64% of the residues. Refinement to 2.3 Å resolution consisted of inspection of electron-density maps and manual model building using *Coot* (Emsley & Cowtan, 2004), followed by positional and *B*-factor restrained refinement with *REFMAC* (Murshudov *et al.*, 1997) to crystallographic $R_{work}$ and $R_{free}$ values of 16.9% and 23.7%, respectively. The occupancy values of the bound iodides were refined using *SHELXL* (Sheldrick & Schneider, 1997) and were manually adjusted based on temperature factor and electron density. Refined occupancy values for the iodide sites ranged from 0.25 to 0.80. The final model includes 304 residues, two $Zn^{2+}$ ions, ten iodides and 203 water molecules. The stereochemistry of the final model was verified using *PROCHECK* (Laskowski *et al.*, 1993; Table 1). Structural superimpositions, structure-based sequence comparisons and all figures were generated using *Chimera* (Pettersen *et al.*, 2004).

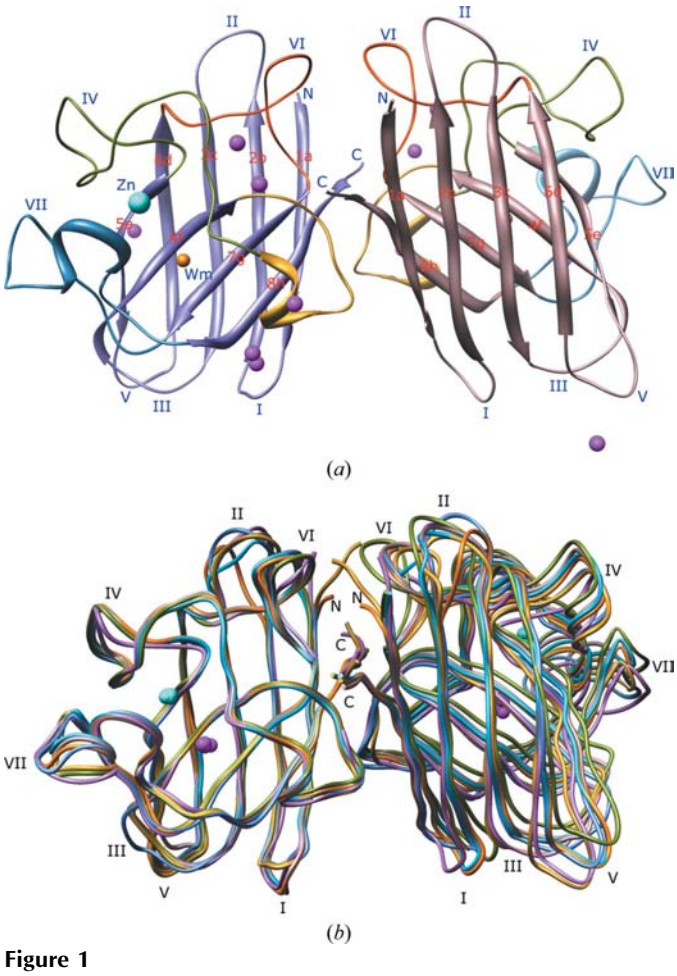


**Figure 1**
(*a*) Structure of Pa-SOD. Each monomer contains an eight-stranded $\beta$-sandwich (1a–8h) with seven loops (I–VII), one short $\alpha$-helix and one $3_{10}$-helix. The disulfide sub-loop comprising residues 50–61 (yellow), metal-binding region 62–83 (green), Greek-key loop 100–113 (orange) and electrostatic loop 119–140 (turquoise) are shown. The bound $Zn^{2+}$, the water molecule (Wm) at the Cu site and iodide ions are represented as cyan, orange and magenta spheres, respectively. The N- and C-termini are marked. (*b*) Pa-SOD (green), So-SOD (purple), Sc-SOD (light blue), Sm-SOD (gold), Xl-SOD (brown), Hs-SOD (deep blue) and Bt-SOD (orange) crystal structures are superimposed onto one monomer (left); the second monomer is in its natural orientation. Bound $Zn^{2+}$ and $Cu^{2+}$ ions are shown as cyan and purple spheres, respectively. The largest conformational difference occurs in the region of electrostatic loop VII.

## 3. Results and discussion

### 3.1. Description of the Pa-SOD structure

The asymmetric unit of the Pa-SOD crystals (space group *C*2) contains two independent molecules of SOD (referred to

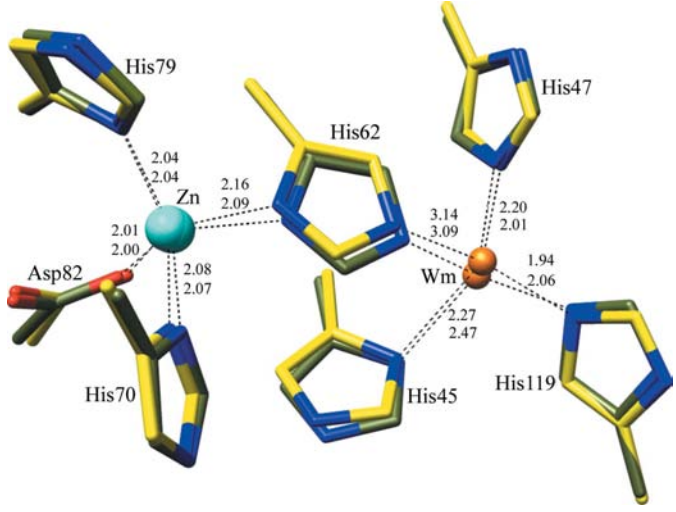


**Figure 2**
Metal-binding residues of Pa-SOD. $Zn^{2+}$ is coordinated by His62, His70, His79 and Asp82. The bound water molecule Wm at the Cu site is held in place by His45, His47, His62 and His119. Ligand-coordination distances for molecules *A* (green) and *B* (yellow) are shown.

in the following as molecules *A* and *B*). The SOD dimer model was therefore generated by a twofold symmetry operation. Each SOD subunit folds into a flattened Greek-key $\beta$-barrel motif consisting of eight antiparallel $\beta$-strands (1a–8h) connected by seven loops (I–VII) (Fig. 1*a*). The active site sits at the bottom of a channel formed by two loops (IV and VII) which extend from the $\beta$-barrel. In Pa-SOD, each subunit contains one zinc ion and one bound water molecule in place of the copper. The single disulfide found in SODs is conserved in Pa-SOD. This S—S bond links loop IV and $\beta$-strand 8h and this linkage of the secondary-structure elements contributes to the stabilization of the SOD fold. The backbone atoms of molecule *A* superimpose well with those of molecule *B* (r.m.s. deviation of ∼0.3 Å). Significant structural differences between molecules *A* and *B* are limited to two regions: the Greek-key loop VI and the electrostatic loop VII. In both molecules *A* and *B*, 18 side chains were modelled with two alternate conformations and nine side chains adopt different conformations. In addition to this, two peptide bonds are flipped at positions 12 and 128. The alternate conformation of Ser72 in subunit *A* is stabilized by hydrogen bonds to the carboxylate groups of Glu74 and Asp75, while in subunit *B* Ser72 is not involved in hydrogen-bond contacts and adopts a single conformation. In molecule *B*, the free Cys95 adopts a double conformation (Supplementary Fig. S1[1]). The coordination sphere of the bound Zn consists of three histidines, His62, His70 and His79, and Asp82. Well defined and continuous electron density is observed for all active-site residues in Pa-SOD. The Zn–ligand distances as well as the distorted tetrahedral coordination geometry are strictly conserved in all CuZnSODs. There is no Cu ion in the present Pa-SOD structure and this may be a consequence of overexpression in *Escherichia coli*, which may lack sufficient amounts of the copper-loading protein (CCS) that is necessary to transfer coppers to SOD. Instead, a bound water molecule (Wm) is found at the Cu-ion site and is coordinated by His45, His47, His62 and His119 (Fig. 2). This bound water molecule (Wm) at the Cu site superimposes well with the high-occupancy Cu sites in Sm-SOD (PDB code 1toa) and in Cu-reduced Bt-SOD (PDB code 1cbj). In Pa-SOD, the distance from the water (Wm) to the $N^{\epsilon 2}$ of the bridging His62 is 3.1 Å, which is comparable with the copper-chelation distances in Sm-SOD and reduced Bt-SOD.

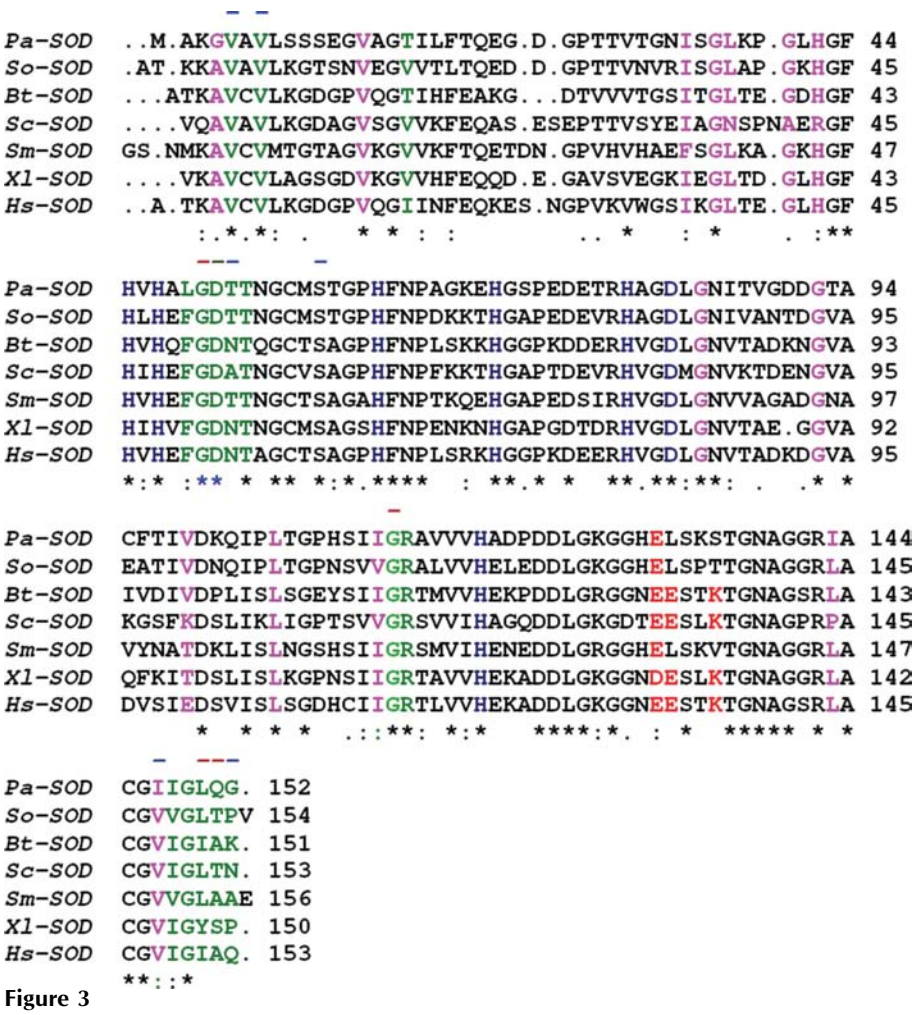


**Figure 3**
Structure-based sequence alignment of eukaryotic CuZnSODs. The proteins are from *Potentilla atrosanguinea* (Pa-SOD), *Homo sapiens* (Hs-SOD), *Bos taurus* (Bt-SOD), *Saccharomyces cervisiae* (Sc-SOD), *Spinacia oleracea* (So-SOD), *Schistosoma mansoni* (Sm-SOD) and *Xenopus laevis* (Xl-SOD). A total of 57 identical/strictly conserved residues, 20 conserved residues and 13 semi-conserved substitutions are marked with asterisks, semicolons and dots, respectively. The $Zn^{2+}$-binding and $Cu^{2+}$-binding active-site residues His and Asp (blue), the dimer-interface residues (green) and the electrostatic guidance residues (red) are shown. Water-mediated main-chain/main-chain, main-chain/side-chain and side-chain/side-chain interactions of the dimer are highlighted by red, green and blue dashed lines. Important familial amyotrophic lateral sclerosis (FALS) mutation sites are shown in magenta.

### 3.2. Comparison with eukaryotic CuZnSOD structures

**3.2.1. Overall conservation and some key differences**. The superposition of backbone atoms of Pa-SOD with various SODs, those from *Bos taurus* (Bt-SOD; PDB code 1cbj; Hough & Hasnain, 1999), *Spinacia oleracea* (So-SOD; PDB code 1srd; Kitagawa *et al.*, 1991), *Saccharomyces cervisiae* (Sc-SOD; PDB code 1sdy; Djinović *et al.*, 1992), *Homo sapiens* (Hs-SOD; PDB code 1azv; Hart *et al.*, 1998), *Xenopus laevis* (Xl-SOD; PDB code 1xso; Carugo *et al.*, 1996) and *Schistosoma mansoni* (Sm-SOD; PDB code 1to4; Cardoso *et al.*, 2004), gives r.m.s. deviations of 0.82, 0.52, 0.71, 0.73, 0.82 and 0.48 Å,

[1] Supplementary material has been deposited in the IUCr electronic archive (Reference: DZ5133). Services for accessing this material are described at the back of the journal.

respectively (Fig. 1*b*). The largest deviations are observed in regions such as (i) the electrostatic loop VII (residues 128–132), (ii) the Greek-key loop VI (residues 100–114) and (iii) the N-terminal segment of the metal-binding loop IV (residues 50–55 and 63–69). The metal ligands (His45, His47, His62, His70, His79, His119 and Asp82) and the S—S bridge (Cys56–Cys145) are conserved in all eukaryotic CuZnSODs (Getzoff *et al.*, 1989; Fig. 3). Furthermore, the residues responsible for maintenance of the active-site geometry (Gly43, Gly60, Pro65, Gly81, Asp123, Gly137 and Gly140) and those important for the stability of the Greek-key structure (Gly15, Leu47, Phe44, Leu105 and Gly146) are also conserved in all eukaryotic CuZnSODs.

In CuZnSODs, Gly is conserved at position 10 in loop I except in the case of Pa-SOD, where Gly is substituted by Ser (Fig. 3). In Pa-SOD, the side-chain $O^{\gamma}$ of Ser10 makes hydrogen-bond interactions with the backbone N atoms of turn residues 12 and 14 as well as with the carbonyl O atom of residue 142. Owing to the presence of Ser10, the $\beta$-strand hydrogen bond between strands 1a and 2b is disturbed. However, an interaction mediated by a water molecule (Wt1) reinforces the $\beta$-strand (Supplementary Fig. S2*a*). The flipping of the carbonyl group of residue 12 (as observed in one molecule of Pa-SOD) is also found in So-SOD, Xl-SOD, Bt-SOD and Hs-SOD (Kitagawa *et al.*, 1991; Carugo *et al.*, 1996; Hough & Hasnain, 1999; Hart *et al.*, 1998). In all SODs two or three water molecules occupy key positions in loop I (five-residue turn), whereas in Pa-SOD these key waters are missing (Supplementary Figs. S2*b* and S2*c*). Thus, interactions mediated by either solvent or side chain (as for Ser10 in Pa-SOD) assist in local stabilization of the protein structure.

In all SODs, the conformation of loop II is stabilized by conserved hydrogen-bonding interactions between Gln22 $O^{\varepsilon 1}$ and Leu105 N and between Gln22 $N^{\varepsilon 2}$ and Gly26 O. In SODs, loop IV (between strands 4f and 5e) is more conserved than some secondary-structure elements ($\beta$-strands 3c and 6f) and does not adopt a defined secondary structure. In fact, loop IV is stabilized by conserved hydrogen-bonding interactions (Supplementary Table 1). In contrast, the electrostatic loop VII of SODs, which is responsible for substrate guidance and attraction, adopts different conformations. This loop is spaced up to ∼2 Å away from the active-site mouth for Pa-SOD, Sm-SOD and So-SOD when compared with Hs-SOD, Bt-SOD, Sc-SOD and Xl-SOD (Fig. 1*b*). This ∼2 Å movement is likely to represent an open conformation of the electrostatic loop.

**3.2.2. Conserved secondary-shell interactions in solution and in crystal structures**. In CuZnSODs, the conformation of the metal-binding site is stabilized by conserved secondary-shell hydrogen bonds (Parge *et al.*, 1992). Details of the hydrogen-bonding interactions are available as supplementary material. These interactions have been observed to be retained in all monomeric/dimeric CuZnSOD studies either in solution or in the crystalline form (Hough & Hasnain, 1999; Kitagawa *et al.*, 1991; Djinović *et al.*, 1992; Carugo *et al.*, 1996; Hart *et al.*, 1998; Banci *et al.*, 1999, 2006; Banci, Bertini, Cantini *et al.*, 2002; Banci, Bertini, Cramaro *et al.*, 2002; Cardoso *et al.*, 2004). The metal-binding residues also have very similar conformations in copper-bound (except for So-SOD) and unbound forms (Kitagawa *et al.*, 1991). These analyses suggest that the site for copper binding remains unchanged even in the absence of $Cu^{2+}$ ions. In most CuZnSODs, the active-site Asp123 acts as a bridge between His45 (Cu ligand), His70 (Zn ligand) and a conserved water molecule (Ws1) (Fig. 4*a* and Supplementary Fig. S3). In So-SOD (Kitagawa *et al.*, 1991), Asp123 adopts a different orientation and Ws1 moves ∼0.5 Å towards the active site. In Sc-SOD (Djinović *et al.*, 1992), the conserved residues His42 and Leu37 are replaced by Arg and Asn, while the secondary-shell hydrogen bonds at the metal-binding site are stabilized by two water molecules (Fig. 4*b*).

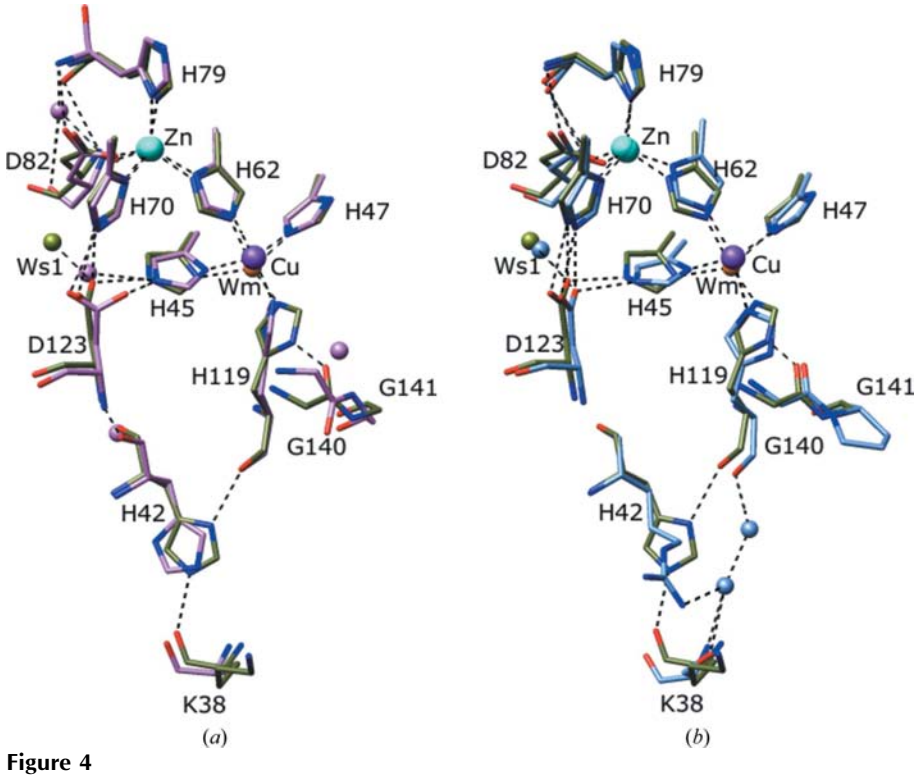


**Figure 4**
Secondary-shell stabilization residues in SODs. (*a*) Pa-SOD (green) superimposed with So-SOD (purple) and (*b*) Pa-SOD with Sc-SOD (light blue). The active sites of Hs-SOD, Bt-SOD, Sm-SOD and Xl-SOD adopt similar geometry to that of Sc-SOD. In all SODs, the metal-ligand residues His45, His47, His62, His70, His79 and Asp82 make similar interactions with their secondary-shell stabilization residues. The structurally conserved water molecule is labelled Ws1.

**3.2.3. Hydrogen-bonding network around the Greek-key loop VI and water molecules around the active site**. In the copper-unbound case of

Pa-SOD, the side-chain N atoms ($N^{\varepsilon}$, $N^{\eta1}$ and $N^{\eta2}$) of Arg114 interact with the carbonyl O atom of residues 48, 108 and 110 (Figs. 5*a* and 5*b*), while in the intermediate and fully copper-loaded states of SODs (as in Sc-SOD, Hs-SOD, Bt-SOD, Xl-SOD and Sm-SOD) there is no direct interaction between Arg114 $N^{\eta1}$ and the carbonyl O atoms of residues 108 and 110 (Djinović *et al.*, 1992; Carugo *et al.*, 1996; Hart *et al.*, 1998; Hough & Hasnain, 1999; Cardoso *et al.*, 2004). However, in the intermediate copper-bound forms of Sc-SOD, Xl-SOD and Sm-SOD, Arg114 $N^{\eta1}$ is linked to the carbonyl O atom of residues 108 and 110 through water W5. In the case of the early bound state (represented by So-SOD), this Arg114 is flipped by 90° (Supplementary Fig. S4). In Pa-SOD, Sm-SOD and Sc-SOD, additional water molecules W1, W1′ and W2 are found and these connect the upper part of the active site with the C-terminal Greek key through a structurally conserved water Ws2. In summary, we observe that in all copper-bound states of SOD (early, intermediate and fully loaded) one or two water molecules (W3 and W4) interact with Arg114. In contrast, no equivalent waters are found in the copper-unbound state of Pa-SOD.

In the copper-unbound and early bound SOD states there is no interaction between the termini of the Greek-key loop VI (Fig. 6*a* and Supplementary Fig. S5). In contrast, inspection of intermediate and fully loaded SOD states reveal interactions of loop VI termini *via* the main-chain O atom of residue 102 and the side-chain N atom of residue 109 (Figs. 6*b* and 6*c*). In the copper-unbound and intermediate states, three or four additional water molecules (W6–W9) are present between loop II and the Greek key (Figs. 6*a* and 6*b*). In all structures, a salt bridge is found between Arg78 and Asp100 and the side-chain $O^{\delta2}$ of Asp100 interacts with the backbone N atom of residue 102. In addition, Asp100 $O^{\delta2}$ also interacts with the backbone N atom of residue 103 in all SODs, with the exceptions of copper-unbound Pa-SOD and early bound So-SOD (Kitagawa *et al.*, 1991; Fig. 6*a* and Supplementary Fig. S5).

In all SODs, both the $N^{\eta1}$ and $N^{\eta2}$ atoms of Arg142 interact with the carbonyl O atom of residue 60. Arg142 $N^{\eta1}$ also interacts with the carbonyl of Cys56 (except in the case of early bound So-SOD; Fig. 7 and Supplementary Fig. S6). In So-SOD, the carbonyl O atom of Gly140 is flipped and His119 adopts different orientations. In the copper-bound intermediate and fully loaded states, there is an interaction between the carbonyl O atom of Gly140 and His119 (Figs. 7*b* and 7*c*). In the copper-unbound and intermediate states of SOD, the active-site channel is filled by six extra water molecules in addition to seven conserved water molecules.

**3.2.4. Dimer interface**. Eukaryotic CuZnSODs are dimeric structures with conserved subunit interfaces. This interface is formed by 16–20 residues emanating from (i) $\beta$-strands 1a, 2b and 8h, (ii) the S—S subloop, (ii) the Greek key and (iv) the C-terminal region. Equivalent residues are provided by the opposing SOD subunit. In eukaryotic CuZnSODs, the residues involved in dimer formation (5, 7, 17, 49–53, 111–113 and 147–151; Fig. 3) are highly conserved throughout evolution. Subunit–subunit recognition is based both on hydrophobic interactions (Ile/Val111, Ile/Val112, Val/Ile147 and Leu/Ile/Tyr150) and on direct hydrogen bonds (Figs. 8*a* and 8*b*). In all CuZnSODs the Val at position 147 is conserved, except in Pa-SOD where the bulkier side chain of Ile is found instead.

There is a significant difference in the relative orientations of the two subunits in CuZnSODs (Fig. 1*b*). Typically, five to eight water molecules form hydrogen bonds and thereby add polar nature to the hydrophobic SOD-dimer interface. Water Ws14 and its equivalent Ws14′ is a structural feature that is conserved in all eukaryotic CuZnSODs. This water is almost completely buried and connects the first and last $\beta$-strands through direct hydrogen bonds to backbone atoms. In Sm-SOD and Hs-SOD (Hart *et al.*, 1998; Cardoso *et al.*, 2004), Ws14 is additionally connected to two other water molecules (Ws13 and Ws15), forming a tetrahedron-like structure (Fig. 8). In the present Pa-SOD, an additional water W10 is present between Ws14′ and Ws15′, although its dimeric partner does not possess an equivalent to W10′.

In Pa-SOD (unbound) and So-SOD (early chelation), a water molecule Ws13 interacts with the carbonyl O atom of Val5 (Fig. 8 and Supplementary Fig. S7). However, in the

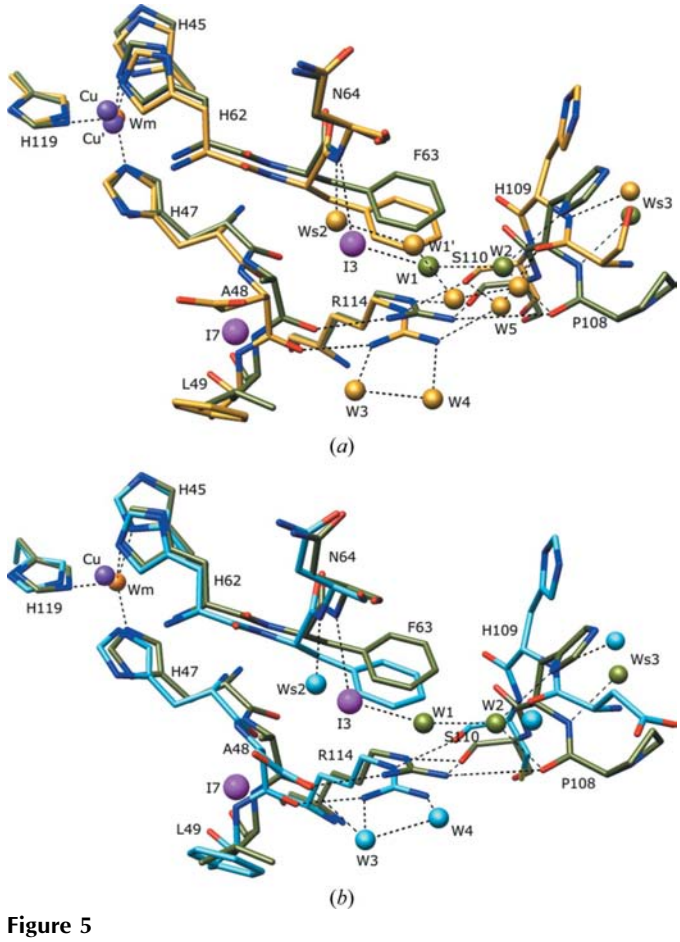


**Figure 5**
Displacement of water molecule Ws2 and residues Phe63 and Arg114 of the C-terminal Greek-key loop. Views are shown of (*a*) copper-unbound Pa-SOD (green) with intermediate-state Sm-SOD (gold) and (*b*) Cu-unbound Pa-SOD with fully loaded Hs-SOD (deep blue). Structural water molecules (Ws2 and Ws3) and additional water molecules (W1–W5) are labelled.

intermediate (Sm-SOD) and fully bound (Hs-SOD) structures this interaction is missing. In all copper-bound forms, the backbone N and O atoms at position 147 interact with Ws14 and Ws15, respectively. In the case of Cu-unbound Pa-SOD, there is no interaction between Ws15 and Ws15′, but in the intermediate and fully loaded states of SODs the two equivalent waters Ws15 do interact.

**3.2.5. The electrostatic loop in CuZnSODs**. In eukaryotic CuZnSODs, the residues involved in electrostatic substrate channelling are essentially located in the loop between $\beta$-strands 7g and 8h, one of the two long loops which extend from the $\beta$-barrel to form the CuZnSOD active centre (Banci *et al.*, 1999). The conserved hydrogen bond between the backbone N atom of His70 and the carbonyl O atom of Lys134 stabilizes the relative conformation of loop IV with loop VII. Residues in the electrostatic loop (131, 132, 135, 136 and the distal Arg142) determine the shape and strength of the electrostatic field around the active site (Tainer *et al.*, 1990). Moreover, these four residues adopt a solvent-exposed hydrogen-bonded helical turn in all CuZnSODs (Tainer *et al.*, 1982; Kitagawa *et al.*, 1991; Djinović *et al.*, 1992; Parge *et al.*, 1992; Carugo *et al.*, 1996; Hart *et al.*, 1998; Hough & Hasnain, 1999; Cardoso *et al.*, 2004). The dismutation reaction is diffusion-limited and the electrostatic loop VII in the active-site channel increases the diffusion rates of superoxide and drives it towards the bound copper and Arg142 (Getzoff *et al.*, 1992).

From Fig. 1(*b*), it is clear that there are large conformational differences of the electrostatic loops between CuZnSODs. This loop (residues 128–132) is ∼2 Å away from the active-site mouth in the cases of Pa-SOD, So-SOD and Sm-SOD (unbound, early and intermediate stages). These structural movements may arise from the open conformation of this loop. Two important charged residues of this loop, Glu132 and Lys135, are replaced by Leu and Ser/Thr/Val in Pa-SOD, So-SOD and Sm-SODs, respectively (Fig. 3). Thus, the entrance to the active site in Pa-SOD and So-SOD is less hydrophobic compared with that in Sm-SOD, but once again does not involve charged residues at these positions as observed in Sc-SOD, Xl-SOD, Hs-SOD and Bt-SOD (Djinović *et al.*, 1992; Parge *et al.*, 1992; Carugo *et al.*, 1996; Hart *et al.*, 1998; Hough & Hasnain, 1999). As mentioned previously, Arg142 interacts with loop IV by forming a hydrogen bond to the carbonyl O atom of Cys57. This hydrogen bond is important in fixing the position of Arg142 in the active-site

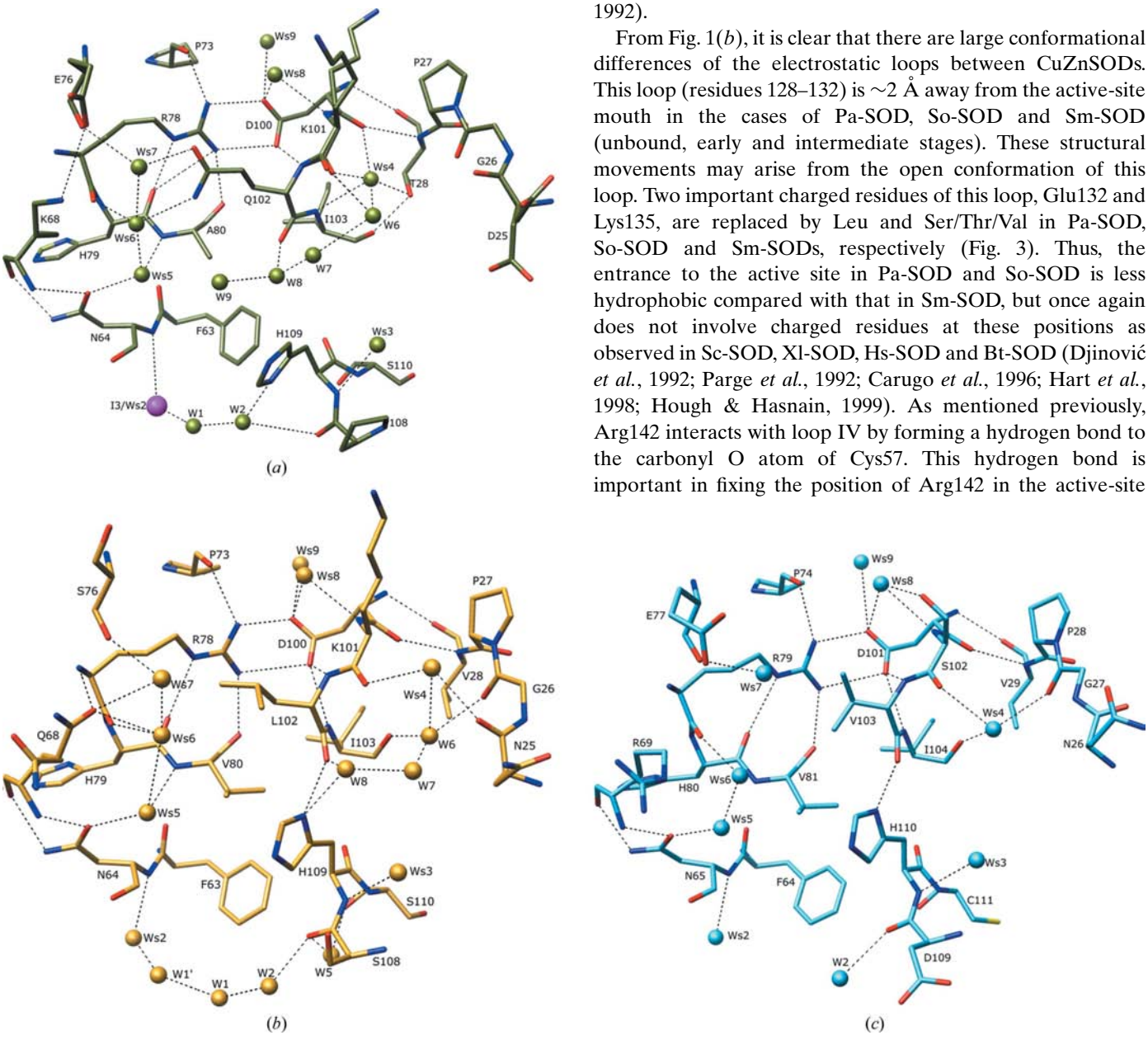


**Figure 6**
Movement of loop II and the Greek-key loop. Views of (*a*) copper-unbound Pa-SOD, (*b*) intermediate-state Sm-SOD (*c*) fully loaded Hs-SOD. There are three to four additional water molecules between loop II and Greek-key loop in the copper-unbound state (Pa-SOD) and in the intermediate state (Sm-SOD).

cavity. The guanidium group of Arg142 has the same conformation in all of the X-ray structures of dimeric CuZnSODs. In the early harbouring state So-SOD (Kitagawa *et al.*, 1991), there is no hydrogen bond between Cys57 and Arg142 (Supplementary Fig. S6*a*). In the electrostatic loop, the carbonyl O atom of Glu/Leu132 is invariantly hydrogen bonded to the backbone N atoms of Thr136 and Ser/Lys135 and to the hydroxyl O atom of Thr136. In the fully copper-loaded state, SODs have hydrogen-bonding interactions between (i) the side-chain $O^{\gamma}$ of Ser133 and both side-chain O atoms ($O^{\delta1}$ and $O^{\delta2}$) of Asp124 and (ii) Asn138 $N^{\delta2}$ and Asp124 $O^{\delta2}$. In contrast, in the unbound, early and intermediate states of SODs (Pa-SOD, So-SOD and Sm-SOD) the side chains of Ser133 and Asn138 have different orientations. The side-chain $O^{\gamma}$ of Ser133 only interacts with Asp124 $O^{\delta2}$ and there is no interaction between residues Asn138 and Asp124.

**3.2.6. Copper-binding process**. Comparative analysis of X-ray and solution structures of SODs shows structural differences in (i) the electrostatic loop (Fig. 1*b*), (ii) the Greek-key loop region (Figs. 5 and 6), (iii) the number of active-site water molecules (Fig. 7) and (iv) the dimer interface (Fig. 8). However, it seems that the copper-chelation site in SODs is pre-built and competent for copper binding even in the absence of the ion and this feature is conserved in all solution and crystal structures.

The following were considered to be hallmarks of the early copper-harbouring stage in SODs: conformational exchange of the copper ligand His119, flipping of the backbone carbonyl O atom in the secondary-shell metal-stabilizing residues (42, 79 and 140), their solvent exposure and a 90° rotation of the Arg114 side arm. In addition, peptide flipping was observed at positions 15, 50, 74, 78, 109, 128 and 130. In the copper-unbound state (as in Pa-SOD), the structurally conserved water molecule Ws2 is replaced by iodide ion I3. A movement of I3 and residue Phe63 were observed in Pa-SOD, just like in the early copper-bound state (So-SOD). Owing to this, Arg114 moves towards the C-terminal Greek key and interacts with the carbonyl O atoms of residues 108 and 110. In contrast to this, in the intermediate and fully loaded states there is no movement observed of Ws2 and Phe63 and furthermore there is no direct interaction between Arg114 and the C-terminal Greek-key loop. However, in the intermediate state water-mediated interactions are found between Arg114 and the C-terminal Greek-key loop. In the unbound and intermediate states, different orientations of residues such as Ser133 and Asn138 induce movement of the electrostatic loop. Rotamer flipping of His109 along with the presence of additional water molecules between loop II and the Greek-key loop induce

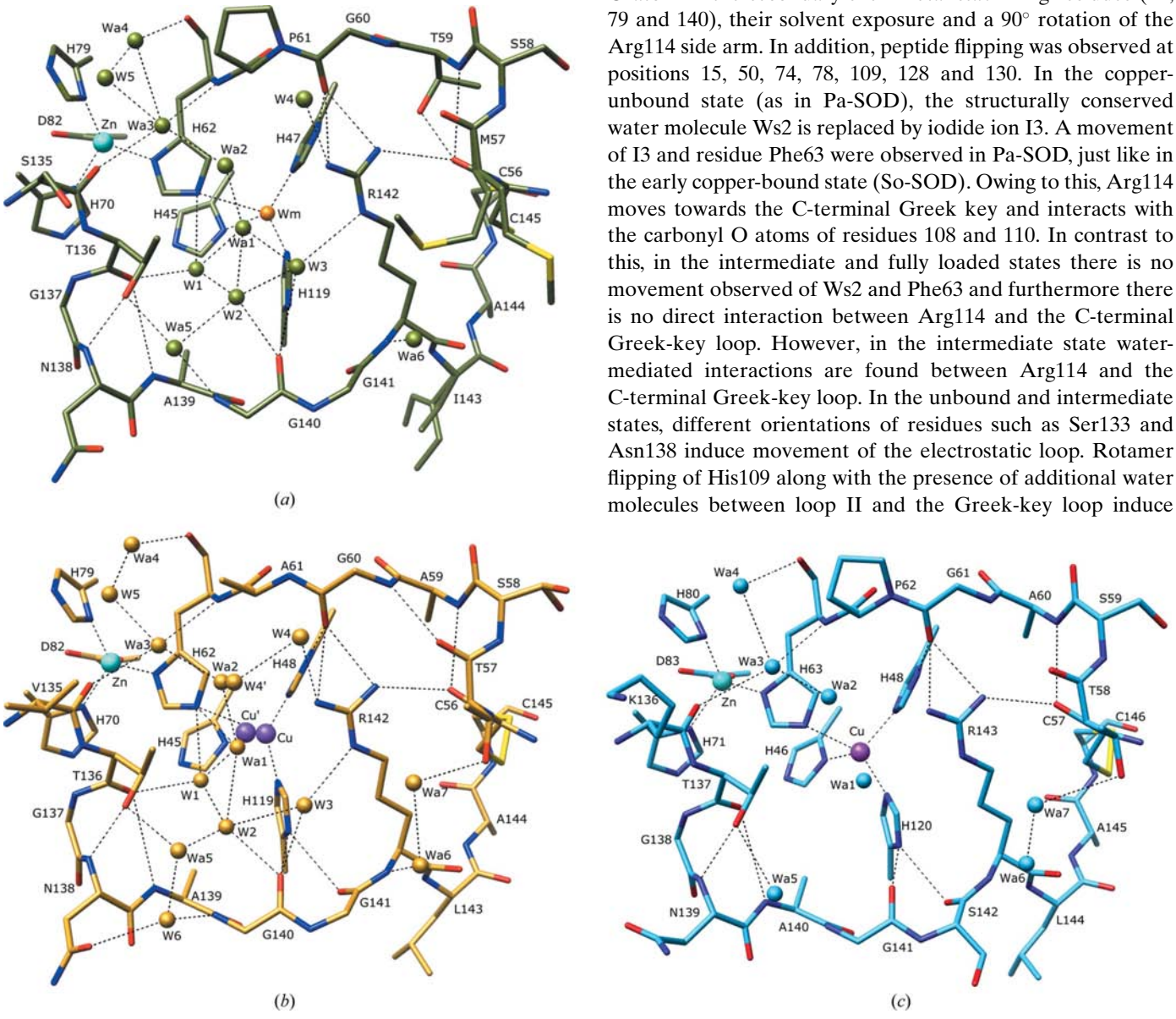


**Figure 7**
Comparison of active-site water molecules in various copper-chelation states. Views are shown of (*a*) Cu-unbound Pa-SOD, (*b*) intermediate-state Sm-SOD and (*c*) fully loaded state Hs-SOD. There are six additional water molecules in Pa-SOD and Sm-SOD compared with the fully loaded state (Hs-SOD).

**Table 2**
Interface and side-chain accessible surface area (ASA).

| | Pa-SOD | So-SOD | Hs-SOD | Sm-SOD | Bt-SOD | Sc-SOD | Xl-SOD |
|---|---|---|---|---|---|---|---|
| Interface accessible surface area | | | | | | | |
| Interface ASA (Å$^2$) | 626.0 | 714.35 | 675.2 | 632.0 | 661.4 | 626.4 | 668.6 |
| Interface ASA (%) | 8.56 | 9.34 | 8.76 | 8.44 | 8.86 | 8.33 | 9.2 |
| Polar atoms (%) | 25.0 | 28.4 | 30.6 | 30.4 | 31.1 | 31.9 | 27.1 |
| Nonpolar atoms (%) | 74.9 | 71.5 | 69.4 | 69.6 | 68.9 | 68.1 | 72.9 |
| Gap volume | 2688.6 | 4251.5 | 4619.0 | 5662.9 | 4007.0 | 4397.3 | 4006.6 |
| Gap volume index | 2.16 | 3.00 | 3.47 | 4.49 | 3.04 | 3.54 | 3.00 |
| Bridging water molecules | 4 | 1 | 3 | 5 | 2 | 2 | 3 |
| Hydrogen bonds | 5 | 6 | 4 | 4 | 4 | 6 | 4 |
| Solvent-exposed side-chain ASA | | | | | | | |
| Total side-chain ASA (Å$^2$) | 6100.1 | 6626.9 | 6706.5 | 6606.6 | 6410.8 | 6606.8 | 6306.3 |
| Basic side-chain ASA (Å$^2$) | 729.9 | 927.7 | 1623 | 1202.6 | 1314.7 | 1312.8 | 1061.3 |
| Basic side-chain ASA (%) | 12.0 | 14.0 | 24.2 | 18.2 | 20.5 | 19.9 | 16.8 |
| Acidic side-chain ASA (Å$^2$) | 1227.1 | 1315.0 | 1498.2 | 1081.5 | 1295.2 | 1474.4 | 1332.5 |
| Acidic side-chain ASA (%) | 20.1 | 19.8 | 22.3 | 16.4 | 20.2 | 22.3 | 21.1 |

movement of the latter. These structural alterations provide a considerable increase in the width of the active-site channel.

We propose that small conformational differences may drive copper binding and these include (i) the conformational exchange of copper-chelating residues, (ii) the flipping of backbone carbonyl O atoms in the secondary-shell metal-stabilizing residues and their solvent exposure, (iii) flipping of Arg114, (iv) movement of the electrostatic loop owing to the different orientations of Ser133 and Asn138, (v) the presence of additional water molecules between the Greek keys and loop II and (vi) rotamer swapping of His109.

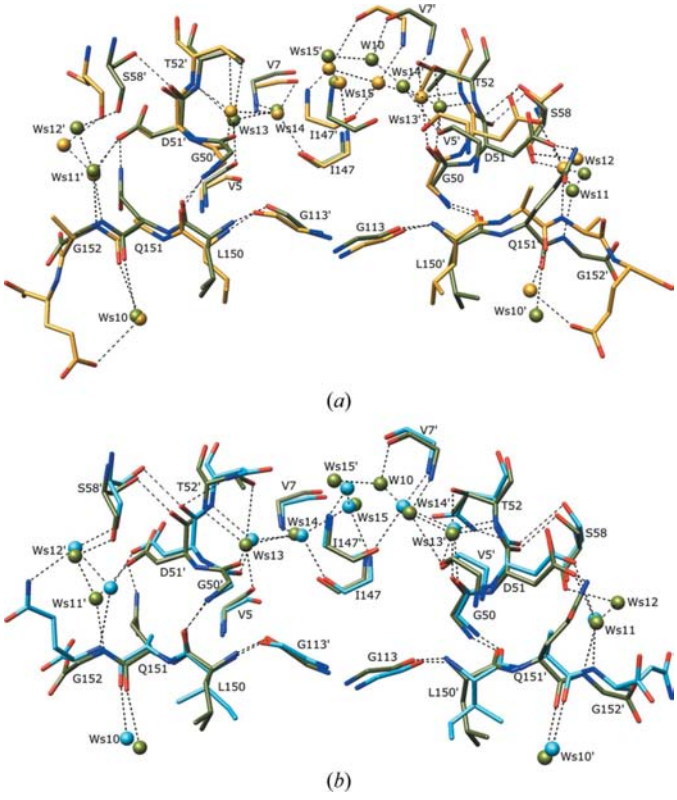


**Figure 8**
View of the symmetric dimer interface. Residues are labelled according to Pa-SOD numbering and the twofold-related molecule is labelled with primes. (*a*) Superposition of Cu-unbound (Pa-SOD) and intermediate states (Sm-SOD) and (*b*) superposition of Cu-unbound (Pa-SOD) and fully copper-loaded states (Hs-SOD). Water molecules and other interactions between the subunits are not superimposable for the Cu-unbound and intermediate states, whereas for the fully copper-loaded state waters and other interactions are superimposable.

### 3.3. Thermostability

SODs are more thermostable (Lepock *et al.*, 1985; Roa *et al.*, 1988) than many other proteins from thermophilic organisms (Stellwagen & Wilgus, 1978). Bt-SOD is stable and remains active in 8 *M* urea (Malinowski & Fridovich, 1979). The Pa-SOD described here is autoclavable at 394 K at a pressure of 1.1 kg cm$^{-2}$ and is stable to boiling in distilled water for 1 h. Analysis of Bt-SOD mutant C6A (McRee *et al.*, 1990) and Hs-SOD mutants C6A and C111S (Parge *et al.*, 1992) demonstrates that intra-loop side chain to main chain interactions and hydrogen bonds can thermodynamically stabilize these enzymes. Cys is conserved at position 6 in SODs from higher organisms, while Ala is conserved in the lower phyla. At position 111, Ser is conserved for most of CuZnSODs except for Hs-SOD, where Ser is replaced by Cys. In the present Pa-SOD, a free Cys is present in $\beta$-strand 4f at position 95 and this position is not conserved in CuZnSODs. This Cys adopts a double conformation in one of the two monomers. At position 10, Gly is conserved for all SODs except in Pa-SOD, where Gly is substituted by Ser (Supplementary Fig. S2), thus displacing several waters which form the hydrogen-bonding network in other CuZnSODs (Fig. 6). This altered hydrogen-bond network arising from Ser10 in Pa-SOD may be partly responsible for its additional stability. Similarly, mutation of the conserved dimer-interface valine (in all SODs) to Ile147 (in Pa-SOD) may contribute to thermostability.

It has been suggested that the occurrence of short loops and proline residues may be responsible for enhanced thermostability (Watanabe *et al.*, 1991). The percentages of proline residues in Pa-SOD, Bt-SOD, So-SOD, Sc-SOD, Hs-SOD, Xl-SOD and Sm-SOD (Tainer *et al.*, 1982; Kitagawa *et al.*, 1991; Djinović *et al.*, 1992; Parge *et al.*, 1992; Carugo *et al.*, 1996; Cardoso *et al.*, 2004) are 5.26, 3.97, 5.84, 5.23, 3.27, 2.67 and 1.92%, respectively, indicating no significant excess of proline residues in Pa-SOD. However, most Pa-SOD prolines are located in $\beta$-turns/loops or are close to the loops and this may contribute to thermostability. Apart from the two conserved prolines in all SODs, the extra prolines in Pa-SOD are replaced by polar/charged residues (such as Glu, Thr/Ser or Lys) in other SODs.

The accessible surface area on dimer formation was calculated for various SODs (Jones & Thornton, 1996; Willard *et al.*, 2003). This was performed by analyzing the gap-volume index between monomers, which represents the complementarity

between subunits. Strikingly, for Pa-SOD this index is the lowest to date (2.16), indicating the smallest gap within the SOD dimer (Table 2). Further, the percentage of nonpolar atoms in Pa-SOD is also the highest amongst structurally described CuZnSODs, suggesting the significance of increased hydrophobicity in thermostability. Finally, in Pa-SOD the fraction of solvent-exposed basic residues is also the lowest (Table 2). These intriguing structural features may underpin the increased thermal stability and higher SOD activity range for Pa-SOD. Incorporation of structural features that enhance thermal tolerance of SODs while retaining their free-radical scavenging abilities may be of utility in protein engineering for a variety of applications.

AS is an International Wellcome Trust Senior Research Fellow in Biomedical Sciences. The X-ray facility at ICGEB is funded by Wellcome Trust, UK. PKB, SD, SK and PSA thank the Department of Biotechnology, Government of India, for funding under the Bioprospection programme.

## References


Adams, P. D., Grosse-Kunstleve, R. W., Hung, L.-W., Ioerger, T. R., McCoy, A. J., Moriarty, N. W., Read, R. J., Sacchettini, J. C., Sauter, N. K. & Terwilliger, T. C. (2002). *Acta Cryst.* D**58**, 1948–1954.

Allen, R. (1995). *Plant Physiol.* **107**, 1049–1054.

Banci, L., Bertini, I., Cantini, F., D'Amelio, N. & Gaggelli, E. (2006). *J. Biol. Chem.* **281**, 2333–2337.

Banci, L., Bertini, I., Cantini, F., D'Onofrio, M. & Viezzoli, M. S. (2002). *Protein Sci.* **11**, 2479–2492.

Banci, L., Bertini, I., Cramaro, F., Del Conte, R. & Viezzoli, M. S. (2002). *Eur. J. Biochem.* **269**, 1905–1915.

Banci, L., Bertini, I., Del Conte, R., Mangani, S., Viezzoli, M. S. & Fadin, R. (1999). *J. Biol. Inorg. Chem.* **4**, 795–803.

Bannister, J. V., Bannister, W. H. & Rotilio, G. (1987). *CRC Crit. Rev. Biochem.* **22**, 111–180.

Bordo, D., Pesce, A., Bolognesi, M., Stroppolo, M. E., Falconi, M. & Desideri, A. (2001). In *Handbook of Metalloproteins*, edited by A. Messerschmidt, R. Huber, T. Poulos & K. Wieghardt. Chichester: John Wiley & Sons.

Cardoso, R. M. F., Silva, C. H. T. P., Ulian de Araújo, A. P., Tanaka, T., Tanaka, M. & Garratt, R. C. (2004). *Acta Cryst.* D**60**, 1569–1578.

Culotta, V. C., Klomp, L. W., Strain, J., Casareno, R. L., Krems, B. & Gitlin, J. D. (1997). *J. Biol. Chem.* **272**, 23469–23472.

Djinović, K., Gatti, G., Coda, A., Antolini, L., Pelsoi, G., Desideri, A., Falconi, M., Marmocchi, F., Rotilio, G. & Bolognesi, M. (1992). *J. Mol. Biol.* **225**, 791–809.

Djinovic Carugo, K., Battistoni, A., Carri, M. T., Polticelli, F., Desideri, A., Rotilio, G., Coda, A., Wilson, K. S. & Bolognesi, M. (1996). *Acta Cryst.* D**52**, 176–188.

Emsley, P. & Cowtan, K. (2004). *Acta Cryst.* D**60**, 2126–2132.

Forest, K. T., Langford, P. R., Kroll, J. S. & Getzoff, E. D. (2000). *J. Mol. Biol.* **296**, 145–153.

Furukawa, Y., Torres, A. S. & O'Halloran, T. V. (2004). *EMBO J.* **23**, 2872–2881.

Getzoff, E. D., Cabelli, D. E., Fisher, C. L., Parge, H. E., Viczzoli, M. S., Banci, L. & Hallewell, R. A. (1992). *Nature (London)*, **358**, 347–351.

Getzoff, E. D., Tainer, J. A., Stempien, M. M., Bell, G. I. & Hallewell, R. A. (1989). *Proteins*, **5**, 322–326.

Hakam, N. & Simon, J. P. (1996). *Physiol. Plant.* **97**, 209–216.

Hart, P. J., Liu, H., Pellegrini, M., Nersissian, A. M., Gralla, E. B., Valentine, J. S. & Eisenberg, D. (1998). *Protein Sci.* **7**, 545–555.

Hough, M. A. & Hasnain, S. S. (1999). *J. Mol. Biol.* **287**, 579–592.

Jones, S. & Thornton, J. M. (1996). *Proc. Natl Acad. Sci. USA*, **93**, 13–20.

Kitagawa, Y., Tanaka, N., Hata, Y., Kusonoki, M., Lee, G., Katsube, Y., Asada, K., Aibara, S. & Morita, Y. (1991). *J. Biochem.* **109**, 447–485.

Kumar, S., Sahoo, R. & Ahuja, P. S. (2002). US Patent 6485950.

Lamb, A. L., Torres, A. S., O'Halloran, T. V. & Rosenzweig, A. C. (2001). *Nature Struct. Biol.* **8**, 751–755.

Laskowski, R. A., MacArthur, M. W., Moss, D. S. & Thornton, J. M. (1993). *J. Appl. Cryst.* **26**, 283–291.

Lepock, J. R., Arnold, L. D., Torrie, B. H., Andrews, B. & Kruuv, J. (1985). *Arch. Biochem. Biophys.* **241**, 243–251.

McRee, D. E., Redford, S. M., Getzoff, E. D., Lepock, J. R., Hallewell, R. A. & Tainer, J. A. (1990). *J. Biol. Chem.* **265**, 14234–14241.

Malinowski, D. P. & Fridovich, I. (1979). *Biochemistry*, **18**, 5055–5060.

Murshudov, G. N., Vagin, A. A. & Dodson, E. J. (1997). *Acta Cryst.* D**53**, 240–255.

Nesbo, C. L., L'Haridon, S., Stetter, K. O. & Doolittle, W. F. (2001). *Mol. Biol. Evol.* **18**, 362–375.

Otwinowski, Z. & Minor, W. (1997). *Methods Enzymol.* **276**, 307–326.

Parge, H. E., Hallewell, R. A. & Tainer, J. A. (1992). *Proc. Natl Acad. Sci. USA*, **89**, 6109–6113.

Pesce, A., Battistoni, A., Stroppolo, M. E., Polizio, F., Nardini, M., Kroll, J. S., Langford, P. R., O'Neill, P., Sette, M., Desideri, A. & Bolognesi, M. (2000). *J. Mol. Biol.* **302**, 465–478.

Pesce, A., Capasso, C., Battistoni, A., Folcarelli, S., Rotilio, G., Desideri, A. & Bolognesi, M. (1997). *J. Mol. Biol.* **274**, 408–420.

Pettersen, E. F., Goddard, T. D., Huang, C. C., Couch, G. S., Greenblatt, D. M., Meng, E. C. & Ferrin, T. E. (2004). *J. Comput. Chem.* **25**, 1605–1612.

Portnoy, M. E., Schmidt, P. J., Rogers, R. S. & Culotta, V. C. (2001). *Mol. Genet. Genomics*, **265**, 873–882.

Roa, J. A., Butler, A., Scholler, D. M., Valentine, J. S., Marky, L. & Breslauer, K. J. (1988). *Biochemistry*, **27**, 950–958.

Sheldrick, G. M. & Schneider, T. R. (1997). *Methods Enzymol.* **277**, 319–343.

Spagnolo, L., Törö, I., D'Orazio, M., O'Neill, P., Pedersen, J. Z., Carugo, O., Rotilio, G., Battistoni, A. & Djinović-Carugo, K. (2004). *J. Biol. Chem.* **279**, 33447–33455.

Stellwagen, E. & Wilgus, H. (1978). *Biochemistry of Thermostability*, edited by S. Friedman, pp. 223–232. Orlando: Academic Press.

Tainer, J. A., Getzoff, E. D., Beem, K. M., Richardson, J. S. & Richardson, D. C. (1982). *J. Mol. Biol.* **160**, 181–217.

Tainer, J. A., Roberts, V. A., Fisher, C. L., Hallewell, R. A. & Getzoff, E. D. (1990). *A Study of Enzymes*, Vol. II, edited by S. A. Kuby, pp. 499–538. New York: CRC Press.

Watanabe, K., Chishiro, K., Kitamura, K. & Suzuki, Y. (1991). *J. Biol. Chem.* **266**, 24287–24294.

Willard, L., Ranjan, A., Zhang, H., Monzavi, H., Boyko, R. F., Sykes, B. D. & Wishart, D. S. (2003). *Nucleic Acids Res.* **31**, 3316–3319.

Yogavel, M., Gill, J., Mishra, P. C. & Sharma, A. (2007). *Acta Cryst.* D**63**, 931–934.